Measurement of the N to Δ Transition Form Factors at low four momentum transfers

A Jefferson Lab Proposal to PAC 50

the NDelta Collaboration

H. Atac (spokesperson), M. Cardona, S. Jia, R. Li, N. Sparveris (spokesperson)[1]
Temple University, Philadelphia, PA 19122, USA

W. Armstrong, S. Joosten, J. Kim, Z.-E. Meziani, C. Peng, P. Reimer, J. Xie, M. Żurek
Argonne National Laboratory, Lemont, IL 60439, USA

A. Camsonne (spokesperson), J.-P. Chen, S. Covrig Dusa, M. Diefenthaler, D.W. Higinbotham
M. K. Jones (spokesperson), D. Mack, M. McCaughan, D. Meekins, B. Sawatzky, G. Smith, A. Tadepalli
Thomas Jefferson National Accelerator Facility, Newport News, VA, USA

M. Paolone (spokesperson), M. Sievert
New Mexico State University, Las Cruces, NM, USA

M. Katramatou, G. Petratos
Kent State University, Kent, OH 44240, USA

W. Lin, R. Gilman, O. Yeung
Rutgers University, Piscataway, NJ 08855, USA

A. Christopher, T. Gautam, M. Kohl, N. Lashley-Colthirst, J. Nazeer, B. Pandey
T. Patel, M. Rathnayake, M. Suresh, L. Tang
Hampton University, Hampton, Virginia 23668, USA

M. Mihovilovič, S. Širca
University of Ljubljana, Slovenia Jožef Stefan Institute, 1000 Ljubljana, Slovenia

N. Kalantarians
Virginia Union University, VA 23220, USA

P. Markowitz
Florida International University, FL USA

[1] contact:sparveri@temple.edu

E. Brash
Christopher Newport University, VA 23606, USA

A. Puckett
University of Connecticut, CT 06269, USA

M. Nycz
University of Virginia, VA 22904, USA

B. Duran
University of Tennessee, Knoxville, USA

D. Androič
University of Zagreb, Zagreb, Croatia

M. Elaasar
Southern University at New Orleans, LA 70126, USA

S. Wood
Old Dominion University, VA 23529, USA

A. Mkrtchyan, H. Mkrtchyan, V. Tadevosyan
A.I. Alikhanyan National Science Laboratory, Yerevan Physics Institute, Armenia

G. Niculescu, I. Niculescu
James Madison University, VA 22807, USA

D. Byer, H. Gao, B. Karki, V. Khachatryan, G. Matousek, E. Nieuwenhuizen
A. Smith, B. Yu, Z. Zhao, J. Zhou
Duke University and Triangle Universities Nuclear Laboratory, NC 27708, USA

Executive Summary

Main Physics Goals: The proposal focuses on the measurement of the $N \rightarrow \Delta$ transition form factors (TFFs) at low four-momentum transfers.

Proposed Measurement: In Hall C, absolute cross sections and azimuthal asymmetry cross section measurements for the $p(e,e'p)\pi^\circ$ reaction will be made at the $\Delta(1232)$ resonance region for Q^2 between 0.015 to 0.055 (GeV/c)^2. The experiment will acquire production data for 8 days and 3 days for optics, normalization and dummy measurements for a total of 11 days of data taking. The TFFs will be extracted from fits to the cross section and the asymmetry measurements.

Specific requirements on detectors, targets, and beam: The HMS will detect protons using the standard detector package. The HMS will run at momentum between 388 to 576 MeV/c and angles of 12.4° to 58.7°. Since the HMS will be detecting low momentum protons that are below the minimum ionizing region typically used in Hall C experiments, the HMS hodoscope operational high voltages will be checked out at the beginning of the experiment. The SHMS will detect electrons using the standard detector package which has the Noble Gas Cherenkov detector replaced by a vacuum exit pipe. The SHMS will run at momentum between 936 to 952 MeV/c and angles of 7.29° to 11.63°. The standard small angle exit beam pipe will be needed. A non-standard beam energy of 1.3 GeV/c ($\pm$ 0.1 GeV/c) is needed and the beam can be unpolarized. The targets will be the standard 4-cm long liquid hydrogen, 4-cm aluminum dummy and optics foil targets. Elastic ep coincidence is needed as measurement of HMS trigger efficiency and check on the HMS momentum optics. For these measurements, The HMS will be at angles of 60.9° to 70.0° and at momentum between 576 to 388 MeV/c while the SHMS will be at angles of 17.3° to 26.3° and at momentum between 1.22 to 1.14 MeV/c.

Previous proposal: This proposal is a follow up to the proposal PR12-21-001 that was submitted to PAC49. Following the recommendation of the PAC49 report, we have resubmitted the proposal with an update to the physics motivation that now focuses on the $N \rightarrow \Delta$ TFFs and we have addressed the technical comments related to the operation of the HMS spectrometer for low momentum protons.

Abstract

The first excited state of the nucleon dominates many nuclear phenomena at energies above the pion-production threshold and plays a prominent role in the physics of the strong interaction. The study of the $N \rightarrow \Delta$ transition form factors (TFFs) allows to shed light on key aspects of the nucleonic structure that are essential for the complete understanding of the nucleon dynamics. With this proposal, we aim to study the TFFs with measurements that will be conducted in Hall C, utilizing the SHMS and the HMS spectrometers, at low four-momentum transfer squared. The experiment will focus on a region where the mesonic cloud dynamics are dominant and rapidly changing. It will provide high precision measurements of the quadrupole TFFs, that have emerged as the experimental signature for the presence of non-spherical components in the nucleon wavefunction and will allow to decode the underlying system dynamics responsible for their existence. The experimental measurements will offer a test bed for chiral effective field theory calculations and benchmark data for the lattice QCD calculations, and will allow to test the theoretical prediction that the Electric and the Coulomb quadrupole amplitudes converge as $Q^2 \rightarrow 0$. The proposed measurements will advance the understanding of baryon structure in QCD and will motivate further theoretical efforts. Moreover, the TFFs enter as an input in a number of scientific topics ranging from the hadronic physics to neutrino oscillation experiments, thus extending further the impact and the scientific merit of the proposed measurements.

1 General considerations

This proposal is a follow up to the proposal PR12-21-001 that was submitted to PAC49. The new proposal has been developed following the recommendation of the PAC49 report, with updates in the discussion of the physics motivation and of the technical questions associated with the detection of low momentum protons with the HMS spectrometer. More specifically:

- In the PAC49 report, the committee asked that we update and resubmit the proposal giving emphasis on the $N \rightarrow \Delta$ transition form factors (TFFs). In the PAC49 summary we read:
  "The PAC regards the proposed measurements of $p \rightarrow \Delta$ transition form factors at very small Q^2 as very interesting." and concludes *"The PAC recommends to change the emphasis of the proposal and invites the proponents to submit a new proposal focusing on $p \rightarrow \Delta$ transitions. This also should be reflected in the title. Such a proposal should emphasize the transition form factor measurements and the direct physics impact they will have."*
  The PAC recommendation is further supported by the PR12-21-001 Theory report (J. Goity and C. Weiss). For the scientific merit of the proposed measurements of the $N \rightarrow \Delta$ TFFs the theory report points out that they will *" ... further enhance the understanding of the baryon structure in QCD."*, *"... would allow one to test the full set of corrections to the large-Nc relations and study the interplay of the two dynamical scales in the baryon form factors."*, *" ... would motivate further theoretical efforts."*.
  Following the above recommendations, and in consultation with theorists, we have greatly revised the physics motivation of the proposal focusing on the $N \rightarrow \Delta$ TFFs and we have updated the title of the proposal accordingly.

- We discuss the technical question related to the operation of the HMS spectrometer for low-momentum protons. This question has been addressed both at the technical and at the simulation level and is discussed in the experimental section of the proposal (Section 3). More specifically: Dedicated studies on the performance of the quadrupole and dipole magnets were conducted with data that were acquired in the 2021 and 2019 running periods. The studies have shown that the HMS can be reliably operated for the low momentum settings of the proposal kinematics. Furthermore, the resolution effects have been explored with simulation studies and the influence on the measured cross sections from all the systematic effects has been quantified. The overall systematic uncertainty on the measured cross sections is found to to be better than 4%. Lastly, we note that the lowest momentum of the 388 (MeV/c) involves only one of the 28 kinematical settings of the proposal. The other 27 settings are above 400 (MeV/c) and involve gradually increasing momenta.

- We have demonstrated the readiness of the experimental and theoretical tools that will be used in the proposed measurements using data from Hall C. More specifically, we have analyzed recent data from the summer 2019 running period in Hall C that were taken parasitically during the E12-15-001 experiment. The data involve the same reaction channel $p(e,e'p)\pi^0$ that is proposed here, and have been acquired using the same experimental setup (SHMS and HMS measuring electrons and protons in coincidence, respectively). The measurements were conducted at a somewhat higher momentum transfer of $Q^2 \sim 0.3$ $(GeV/c)^2$, where the cross section is well known. The cross section results demonstrate that we have an excellent understanding of the coincidence acceptance in the simulation of the experiment, a good handle of the systematic uncertainties, and validate the readiness of all the experimental and theoretical tools involved in the analysis of the proposed measurements.

2 Introduction

2.1 Physics motivation

The first excited state of the nucleon dominates many nuclear phenomena at energies above the pion-production threshold and plays a prominent role in the physics of the strong interaction. The study of the transition form factors in-turn has allowed the exploration of various aspects of the nucleonic structure. Hadrons are composite systems with complex quark-gluon and meson cloud dynamics that give rise to non-spherical components in their wavefunction, which in a classical limit and at large wavelengths will correspond to a "deformation"[1–4]. The determination and subsequent understanding of the shapes of the fundamental building blocks in nature is a particularly fertile line of investigation for the understanding of the interactions of their constituents amongst themselves and the surrounding medium. For hadrons this means the interquark interaction and the quark-gluon dynamics. For the proton, the only stable hadron, the vanishing of the spectroscopic quadrupole moment, due to its spin 1/2 nature, precludes access to the most direct observable of deformation. As a result, the presence of the resonant quadrupole amplitudes $E_{1+}^{3/2}$ and $S_{1+}^{3/2}$ (or E2 and C2 photon absorption multipoles respectively) in the predominantly magnetic dipole $M_{1+}^{3/2}$ (or M1) $\gamma^* N \rightarrow \Delta$ transition has emerged as the experimental signature for such an effect[1–43]. Nonvanishing quadrupole amplitudes will signify that either the proton or the $\Delta^+(1232)$ or more likely both are characterized by non-spherical components in their wavefunctions. These amplitudes have been explored up to four momentum transfer squared $Q^2 = 6\ (GeV/c)^2$ [8–16,16–24,30–36] (see Fig. 1) and the experimental results are in reasonable agreement with models invoking the presence of non-spherical components in the nucleon wavefunction. The relative strength of the $E2$ and $C2$ amplitudes is normally quoted in terms of their ratio to the dominant magnetic dipole, namely through the EMR and CMR ratio respectively.

In the constituent-quark picture of hadrons, the non-spherical amplitudes are a consequence of the non-central, color-hyperfine interaction among quarks[2,6]. However, it has been shown that this mechanism only provides a small fraction of the observed quadrupole signal at low momentum transfers, with the magnitudes of this effect for the predicted E2 and C2 amplitudes[7] being at least an order of magnitude too small to explain the experimental results and with the dominant M1 matrix element being $\approx 30\%$ low. A likely cause of these dynamical shortcomings is that such quark models do not respect chiral symmetry, whose spontaneous breaking leads to strong emission of virtual pions (Nambu-Goldstone Bosons)[5]. These couple to nucleons as $\vec{\sigma} \cdot \vec{p}$ where $\vec{\sigma}$ is the nucleon spin, and $\vec{p}$ is the pion momentum. The coupling is strong in the p wave and mixes in non-zero angular momentum components. Based on this, it is physically reasonable to expect that the pionic contributions increase the M1 and dominate the E2 and C2 transition matrix elements in the low Q^2 (large distance) domain. This was first indicated by adding pionic effects to quark models[37–39], subsequently in pion cloud model calculations[26,27], and recently demonstrated in Chiral Effective Field Theory calculations[40]. With the existence of these non-spherical amplitudes well established[4], recent high precision experiments and theoretical efforts have focused on testing in depth the reaction calculations and on decoding the underlying nucleon dynamics. The proposed measurements focus on the low momentum transfer region, where the mesonic cloud dynamics is predicted to be dominant and rapidly changing (e.g. see Fig. 2 and Fig. 3), offering a test bed for chiral effective field theory calculations and benchmark data for the lattice QCD calculations. Moreover, the new measurements will allow to test the theoretical prediction that the Electric and the Coulomb quadrupole amplitudes converge as $Q^2 \rightarrow 0$. The merit of the proposed measurements extends further to a number of scientific problems in hadronic and neutrino physics, where the $N \rightarrow \Delta$ TFFs enter as an input.

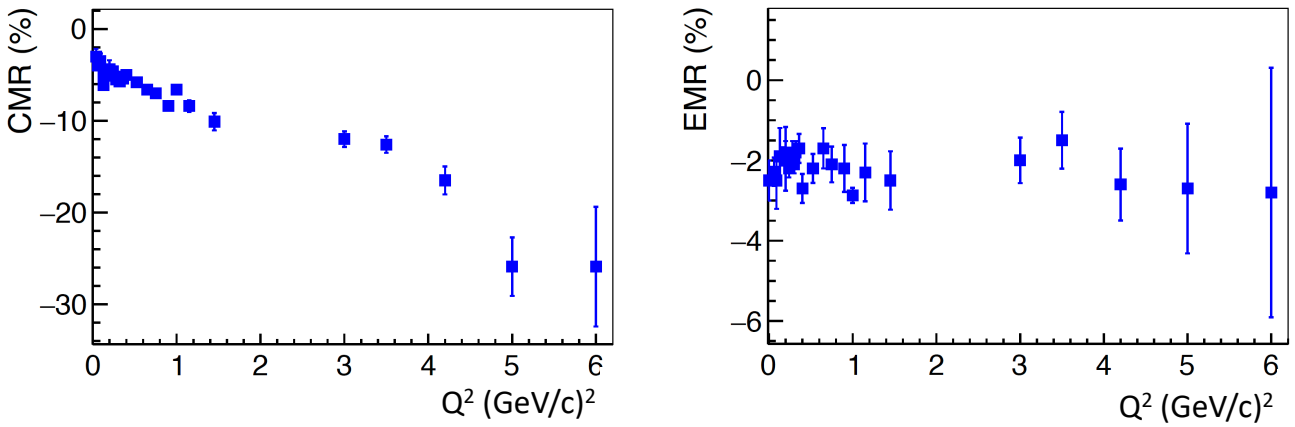

Figure 1. The world data[8–16, 16–24, 30–36] for the CMR and the EMR ratios.

2.1.1 Theoretical descriptions of the $\gamma^*N\Delta$ transition and impact of the propsed measurements

A first theoretical description of the predominantly magnetic dipole ($M1$) $\gamma^*N\Delta$ transition can be achieved founded on symmetries of QCD and its large number-of-color (N_c) limit where the baryon sector formed of up, down, and strange quark flavors displays an $SU(6)$ spin-flavor symmetry. The spin-flavor global symmetry of QCD is at the foundation of many quark models, in which baryons are described as non-relativistic quantum-mechanical three-quark system moving in a confining potential. Within this framework, the $N \to \Delta$ transition is described by an $M1$ spin flip of a quark in the S-wave state. The SU(6) symmetry allows to relate the magnetic dipole moments of the proton and the $p \to \Delta^+$ transition as $\mu_{p\to\Delta^+} = 2\sqrt{2}/3\,\mu_p = 2.63\,\mu_N$ (that falls somewhat short compared to the experimentally derived[48] $\mu_{p\to\Delta^+} = [3.46 \pm 0.03]\,\mu_N$) , while a D-wave admixture in the nucleon or the Δ wave functions allows non-zero values for the $E2$ and $C2$ quadrupole transitions. In the early quark model of Isgur-Karl[49] the constituent quarks move in a harmonic oscillator type long-range confining potential, which is supplemented by an interquark force corresponding with one-gluon exchange. This one-gluon exchange leads to a color hyperfine interaction - which was found to predict well the mass splittings between octet and decuplet baryons[50] - and contains a tensor force which produces a D-state admixture in the N and Δ ground states of about 1 % [51,52]. As a consequence of such D-wave components, the N and Δ charge densities become non-spherical, resulting to small negative values in the sub-percent level for the EMR. Despite the success of the simplistic constituent quark model in predicting the structure and spectrum of low-lying baryons, it under-predicts $\mu_{N\to\Delta}$ by about 25 % and accounts for an EMR amplitude that is smaller by an order of magnitude compared to the experimental values. As a general consideration, the constituent quark models do not satisfy the symmetry properties of the QCD Lagrangian. The *chiral symmetry* is spontaneously broken in nature leading to the appearance of massless Goldstone modes (pions) which acquire a mass due to the explicit breaking of chiral symmetry. Being the lightest hadrons, the pions dominate the long-distance behavior of hadron wave functions and become particularly relevant in the $\Delta(1232)$ resonance that decays dominantly into πN. As such, a logical step is to include pionic degrees of freedom in order to qualitatively improve on the constituent quark models. Such efforts to integrate pionic effects in the N-Δ transition involved e.g. the chiral bag model[53,54], the Skyrme models[55,56], where the nucleon appears as a soliton solution of an effective non-linear meson field theory, the chiral quark soliton model (χQSM), which interpolates between a constituent quark model and the Skyrme model[57], etc. Other efforts based on quark models have restored chiral symmetry by including two-body exchange currents between the quarks, that lead to non-vanishing $\gamma^*N\Delta$ quadrupole amplitudes[58] even if the quark wave

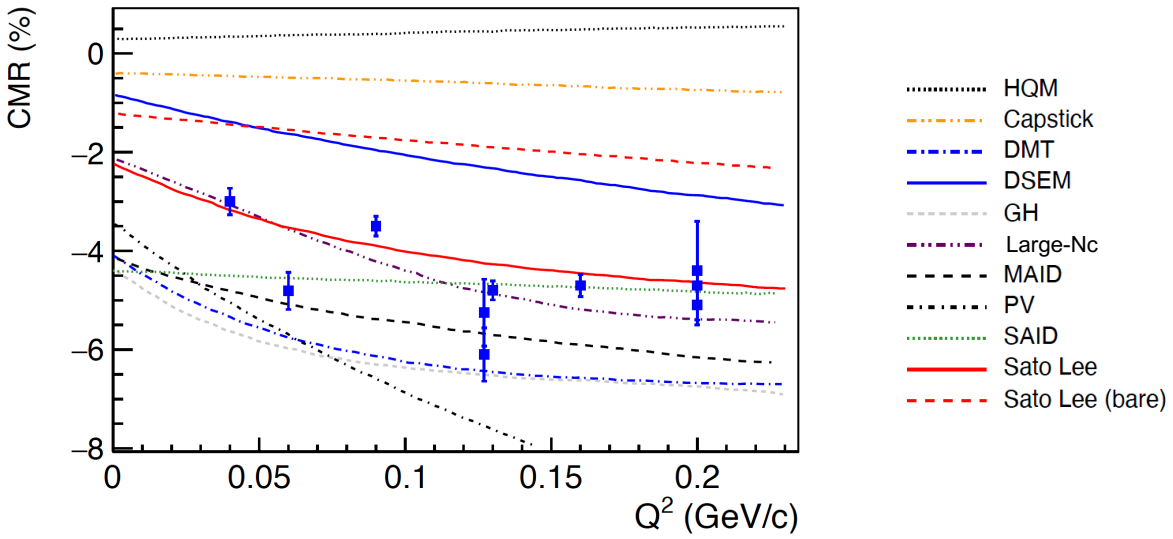

Figure 2. The world data and the theoretical calculations[7,26–28,40–42,44–47] for the Coulomb quadrupole to magnetic dipole transition form factors ratio at low Q^2. The data points are shown with the total experimental uncertainties (statistical and systematic) added in quadrature.

functions have no D-state admixture. In this type of hybrid quark & pion cloud models the non-zero values of the intrinsic quadrupole moments arises purely from the pion cloud. In the model of[58] the Δ is excited by flipping the spins of two quarks resulting to an EMR $\simeq -3.5\%$. The model also relates the $N \to \Delta$ and Δ^+ quadrupole moments to the neutron charge radius as $Q_{p\to\Delta^+} = r_n^2/\sqrt{2}$ and $Q_{\Delta^+} = r_n^2$. Using the experimental value for the neutron charge radius one derives from the above relation $Q_{p\to\Delta^+} = -0.08$ fm^2 that agrees well with the extracted value[48] for $Q_{p\to\Delta^+}$.

In order to obtain results that are more directly related to QCD, one can follow theoretical approaches such as the $1/N_c$ expansion of QCD (limit of large number of colors), chiral effective field theory (chiral limit of small pion masses or momentum transfers) or lattice QCD simulations (continuum limit). The $1/N_c$ expansion of QCD[59,60] offers an expansion with a perturbative parameter at all energy scales and has proved quite useful in describing properties of baryons, such as, ground-state and excited masses, magnetic moments, and electromagnetic decays[61,62]. For the $N \to \Delta$ transition, the magnetic moment $\mu_{N\to\Delta}$ is related to the isovector nucleon magnetic moment as[63] $\mu_{p\to\Delta^+} = (\mu_p - \mu_n)/\sqrt{2} \simeq 3.23\,\mu_N$ that agrees within 10 % of the experimentally derived value and the EMR value is shown to be of order $1/N_c^2$[64] thus offering a physical explanation of its magnitude in the large N_c limit. The relation $Q_{p\to\Delta^+} = r_n^2/\sqrt{2}$ that was discussed above was also shown[65] to hold in the large N_c limit. Furthermore in the large N_c limit it was shown[66] that at $Q^2 = 0$ the EMR $= (1/12)\, R_{N\Delta}^{3/2}\, (M_\Delta^2 - M_N^2) r_n^2/\kappa_V$ where $R_{N\Delta} \equiv M_N/M_\Delta$, and $\kappa_V = \kappa_p - \kappa_n$ is the isovector nucleon anomalous magnetic moment. The large N_c prediction yields EMR $= -2.77\,\%$ that is in excellent agreement with the experimental measurement for EMR. In the case of CMR, where a direct measurement at the real-photon point is not possible, extending the large-N_c relation to finite Q^2 leads to relations with the neutron electric form factor, which agree remarkably well with the experimental measurements[66,67].

Lattice QCD offers a direct path to calculate the N to Δ transition form factors starting from the underlying theory of QCD. The LQCD calculations[25,68] have been preformed so far with pion mass down to $\sim 300\ MeV$, where the Δ is still stable. These results tend to somewhat underestimate the M1, similarly to what has been observed in results for the nucleon EM form factors. Such effects can be further

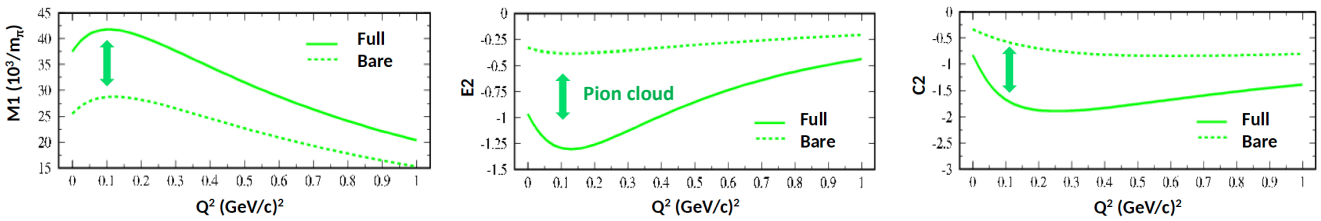

Figure 3. The effect of the pion cloud to the resonant amplitudes as predicted by the Sato Lee calculation (Bare: without the pion cloud).

investigated through lattice calculations with smaller pion masses. The LQCD results for EMR and CMR on the other hand exhibit remarkable agreement with the experimental measurements, pointing to the fact that the ratios are much less affected by lattice artifacts than each of the quantities separately. The statistical uncertainties of the early LQCD results for the two ratios are somewhat large due to the fact that the two quadrupole amplitudes are sub-dominant and more challenging to determine. Nevertheless, recent progress enables LQCD calculations nowdays to be conducted with physical pion mass, and with statistical uncertainties that are comparable to the experimental ones, thus making the need for new experimental measurements timely and extremely important. More specifically, the Δ-resonance is currently being investigated by the Extended Twisted mass Collaboration[69] using such gauge ensembles within the Luscher approach[70]. Calculations focusing on the Δ-resonance will be the next target using the same formalism developed for rho-meson[71] with the expectation that in the next couple of years lattice calculations of the transition form factors will emerge with much better controlled systematics. In Fig. 4 Lattice QCD results offer geometrical insight to the nucleon through calculations of the three-dimensional contour plot of the Δ^+[72] and of the Δ^+ quark transverse charge density[73].

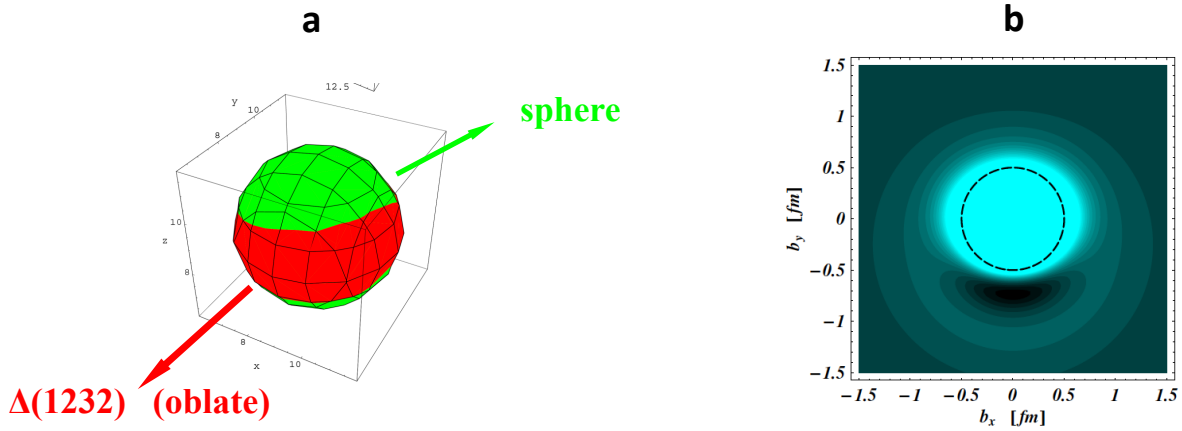

Figure 4. Lattice QCD results of the three-dimensional contour plot of the Δ^+[72] and of the Δ^+ quark transverse charge density[73].

Another path to approach the physics of interest involves the chiral effective field theory (χEFT). It provides a firm theoretical framework at low scales, with the relevant symmetries of QCD built in consistently. The N to Δ transition presents a challenge for χEFT as it involves the interplay of two light mass scales, the pion mass and the $N-\Delta$ mass difference. Studies, taking into account these two

mass scales, have been performed within the framework of heavy-baryon chiral perturbation theory[74] or the more comprehensive study carried out[75,76] using the "ε-expansion" scheme. In the latter, the two scales, the pion mass $\varepsilon \equiv m_\pi/\Lambda_{\chi\mathrm{SB}}$ (with $\Lambda_{\chi\mathrm{SB}} \sim 1$ GeV the chiral symmetry breaking scale) and the Δ-resonance excitation energy $\delta \equiv (M_\Delta - M_N)/\Lambda_{\chi\mathrm{SB}}$ are counted as being of the same order, namely $\varepsilon \sim \delta$. The "δ-expansion" scheme has been introduced[77] to provide an energy-dependent power-counting scheme that takes into account the large variation of the Δ-resonance contributions with energy, and treats the two light scales ε and δ on a different footing, counting $\varepsilon \sim \delta^2$, the closest integer-power relation between these parameters in the real world. It has been applied to the study of the N to Δ transition form factors[78] and has been used to extrapolate the current lattice QCD calculations to the physical pion mass, reconciling the lattice results and the experimental values for the CMR.

The study of the N to Δ transition, one of the central components of Jefferson Lab's research program for many years, has involved a vibrant activity from a large number of experiments in three experimental halls (A, B and C) as seen in Fig. 1. In parallel, the experimental effort has been complemented by a strong theoretical component, as seen in Fig. 2. The improved precision, strong constraints, and extended kinematical reach of the proposed measurements will allow to study the quadrupole transition form factors to a level that would further enhance the understanding of baryon structure in QCD and would motivate further theoretical efforts.

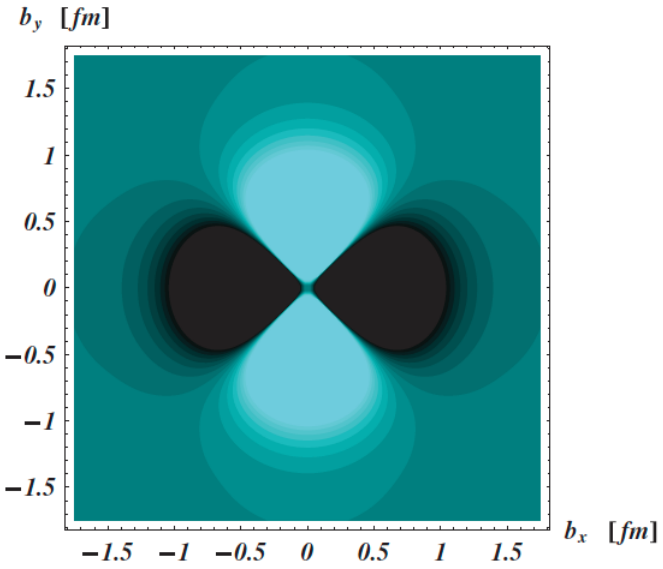

Figure 5. Quadrupole contribution to the transverse charge density for the $N \to \Delta$ transition[79], when N and Δ are polarized along the x axis with spin projection +1/2.

The measurement of the $N \to \Delta$ TFFs allows a link between the underlying dynamics of the nucleon, as seen e.g. in Fig. 3, and the spatial representation of the transition charge density which induces the $N \to \Delta$ excitation[79] as viewed from a light front moving towards a transversely polarized nucleon. This transition charge density contains both monopole, dipole and quadrupole patterns. The quadrupole pattern shown in Fig. 5 maps the spatial dependence in the deformation of the transition charge distribution.

The scientific merit of the proposed measurements can be further identified in the context of the large N_c relations between the elastic and the transition form factors of the nucleon[66]. These relations have

been successful and valuable in providing information for the elastic form factors from experimental measurements of the N-Δ TFFs[80] (see Fig. 6). This can be particularly useful in kinematical regions where the measurements of the nucleon elastic form factors face experimental limitations. The relations receive significant corrections that can be analyzed and confronted with data. Such corrections arise from the conventional $1 / N_c$ expansion and from corrections that involve the pion mass as a dynamical scale and are expected to become important at lower Q^2. These corrections could be analyzed in a theoretical framework that combines Chiral Perturbation Theory with the $1/N_c$ expansion[81]. Measurements of the N to Δ transition form factors at $Q^2 \sim 10^{-2}$ GeV^2 would allow one to test the full set of corrections to the large-N_c relations and study the interplay of the dynamical scales in the baryon form factors.

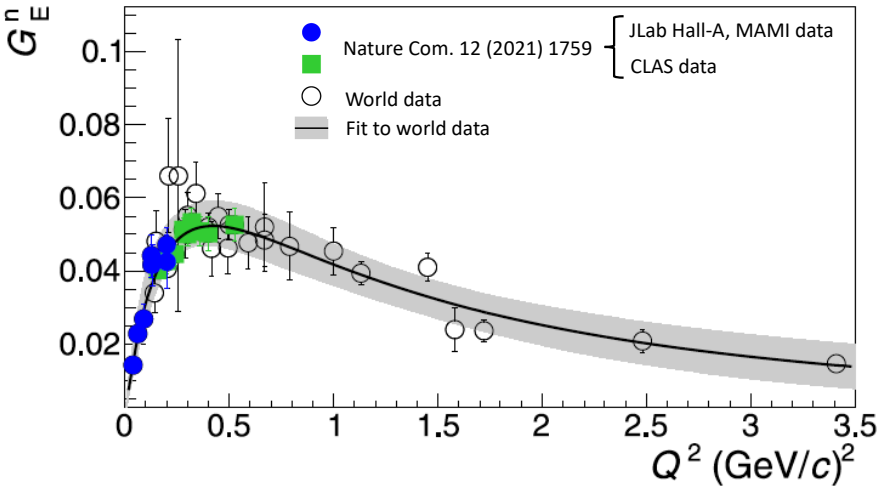

Figure 6. The world data for G_E^n are shown as open symbols. The extraction of G_E^n from the experimental measurements of the $N \rightarrow \Delta$ transition form factors[80] is shown with the filled (blue, green) symbols.

Various key dynamical aspects of the nucleon are naturally related to each other quite closely. On that basis, high precision measurements of the N→ Δ transition form factors carry scientific value since they enter as input parameters in a number of scientific problems. One such example involves the measurement of the electromagnetic Generalized Polarizabilities (GPs) of the proton[82]. The GPs characterize the proton's response to an external electric or magnetic field, and describe how easily the charge and magnetization distributions in the nucleon are distorted by the EM field as a function of the distance scale within the system. The polarizabilities are sensitive to the excited spectrum of the nucleon. That is quite different compared to the nucleon elastic form factors that describe only the ground state of the system. The extraction of the GPs is particularly beneficial when the measurements of the VCS reaction are conducted in the nucleon resonance, compared e.g. to measurements that access the pion production threshold region, as has been previously exhibited e.g. in[83,84]. In order to extract the GPs from the experimental measurements in the Δ region, the analysis of the VCS cross sections is conducted in the context of Dispersion Relations[85–87], where the transition form factors enter as an input. The accurate description of the transition form factors becomes thus important for the precise extraction of the proton GPs. This is particularly relevant at low-Q^2 where we are currently facing a puzzle in explaining the behaviour of the electric polarizability[82], as well as challenges with the precision of the experimental measurements when it comes to decoding the interplay of the competing paramagnetic and diamagnetic contributions in the proton, within a rapidly changing dynamical region.

The relevance of the Δ-resonance extends to neutrino oscillation experiments that focus on the study

of the neutrino mass hierarchy and of the leptonic CP violation. The precise interpretation of these data requires a reliable understanding of neutrino-nucleus reactions[88,89], since the neutrinos are identified through the remnants of these reactions. The neutrino energy relevant to the oscillation experiments spans from several hundred MeV to a few GeV. This requires that the neutrino-nucleus reactions are well understood over a wide kinematical region where the dominant reaction mechanisms tend to vary across the quasi-elastic, resonance and deep inelastic regions. For relatively low energy neutrinos at the ~ 1 *GeV* range the Δ-resonance becomes particularly important. During the process, the internal structure of a scattered nucleon is excited to a resonant state that in-turn decays into a meson-baryon final state, where the meson-baryon dynamics play a central role. In extracting the neutrino properties from the experimental measurements, a dominant source of systematic error involves the uncertainties in neutrino-nucleus reaction cross sections. These contributions have to be understood with an accuracy at the few percent level in order to meet the objectives of the neutrino oscillation experiments. In addressing these uncertainties and reducing them to the desired level, a synergistic effort is required that combines precise experimental measurements in the Δ-resonance, nuclear theorists and neutrino experimentalists.

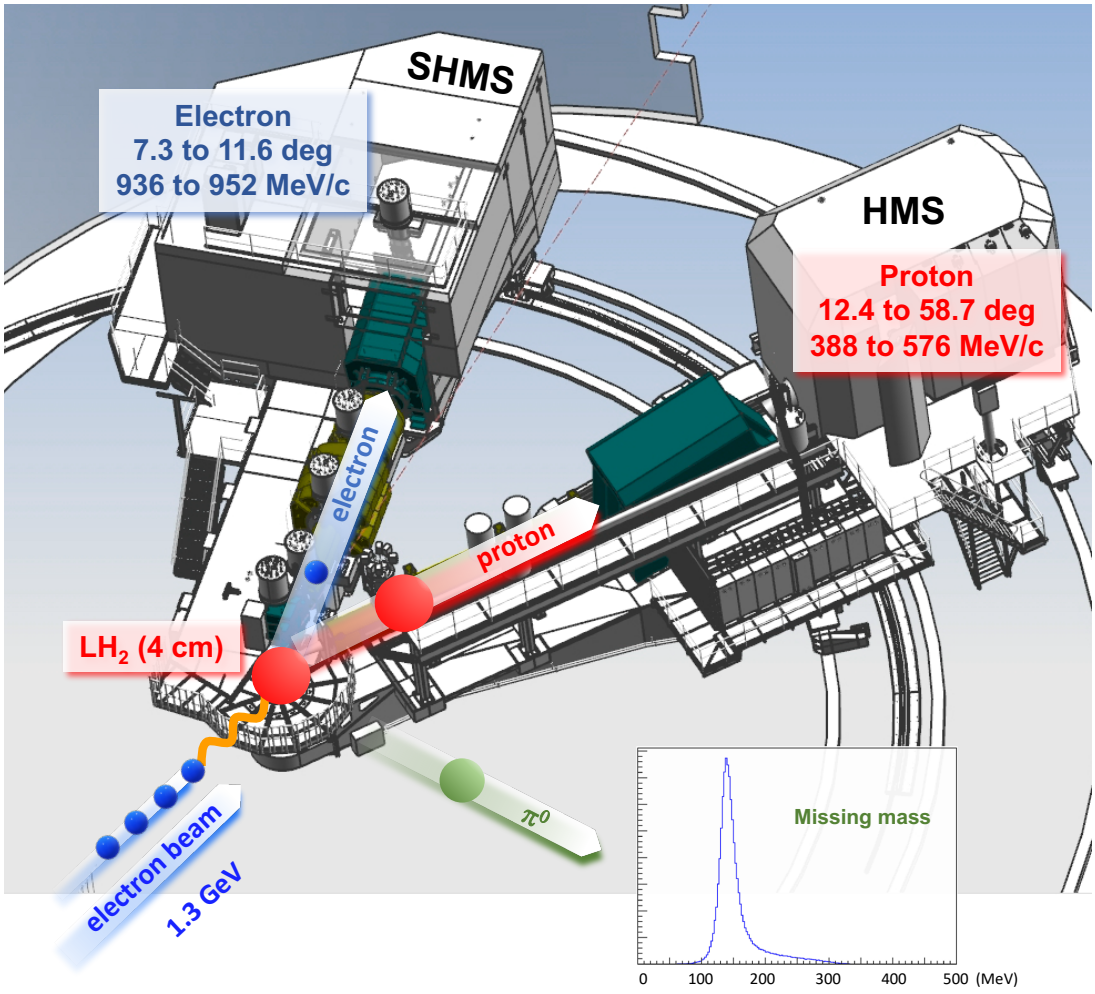

Figure 7. An illustration of the experimental hall and the proposed kinematic settings in Hall-C. See Tab. 1 for exact central angle and central momentum settings for each spectrometer arm.

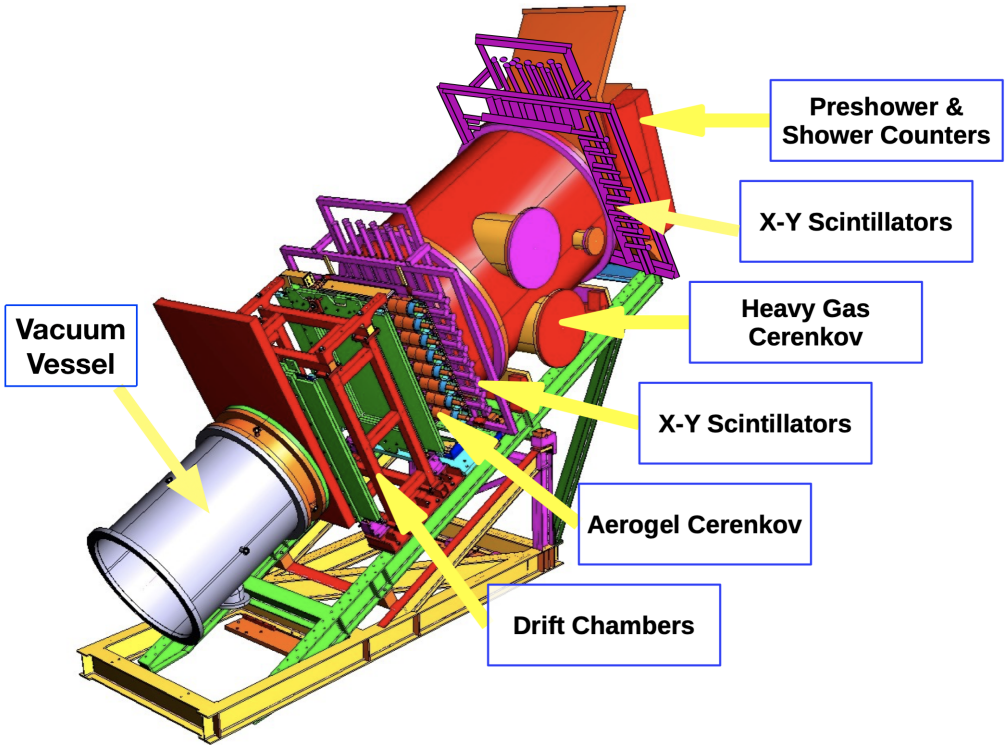

Figure 8. HMS Detector stack.

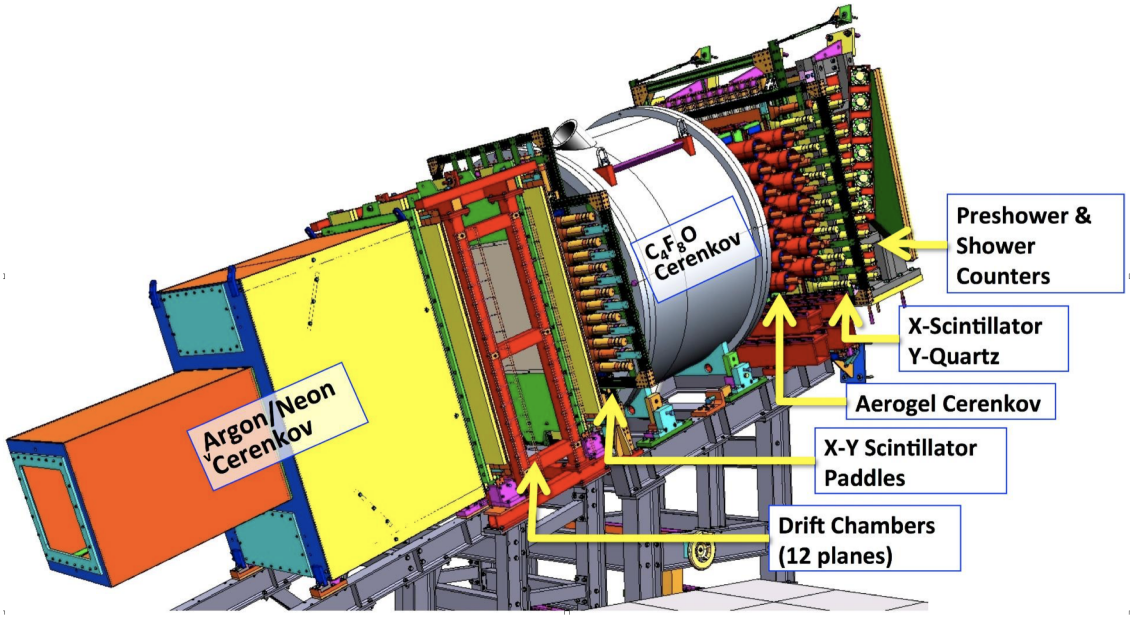

Figure 9. SHMS Detector stack. For this experiment, the standard SHMS configuration in which the Argon/Neon Cerenkov is replaced with a vacuum pipe will be used.

3 The Experiment

3.1 Experimental apparatus and set-up

The experiment will involve measurements of the $p(e,e'p)\pi^0$ reaction. In an experimental arrangement as shown in Fig. 7, the SHMS and the HMS will detect electrons and protons, respectively. The undetected pion will be identified through the missing mass reconstruction. The spectrometers will employ their standard detector packages which are shown in Fig. 8 and Fig. 9 for the HMS and SHMS. For the SHMS, the Argon/Neon Cerenkov would be replaced by a vacuum pipe which is an additional standard SHMS detector stack configuration. This will reduce the multiple scattering before the SHMS drift chambers and improve the missing mass resolution. The target requested is a 4 cm LH2 cell, and the beam current will be ranging from 6 μA (for the lowest-Q^2 setting) to 15 μA. With the small expected π^- to electron rate (see Table 2) the calorimeter alone in the SHMS will provide all the needed π^- from electron separation. With the proton's momenta under 1.0 GeV/c, timing information will be more than sufficient to separate protons from π^+'s in the HMS. Dedicated optics runs will be required for the SHMS spectrometer since it will acquire data in momenta around 1 GeV/c. A set of elastic runs will be taken for calibration and normalization purposes. The beam energy required is 1.3 GeV for all kinematic settings.

Considering the low momentum protons in the HMS, the coincidence time difference between the two spectrometers will vary from 90 ns to 170 ns as the proton momentum varies from 570 to 380 MeV/c. The experiment will change the timing between the two arms at the trigger for each kinematic setting accordingly, to center the HMS trigger within the SHMS trigger window. We plan to run with the SHMS trigger window with width of 60ns and the HMS trigger window width of 20ns. At HMS central momentum of 388 MeV/c, the protons at the large negative delta region will stop in the last scintillator plane. The protons are far away from minimum ionizing region and the pulse heights in the scintillators will be larger than typically seen in Hall C experiments. We plan on running the HMS scintillators at lower high voltages and determining the optimal HV for running at this low momentum. The trigger efficiency will be determined with elastic singles and coincidence data between the electron and proton, throughout the momentum range of the experiment.

A technical point involves the stability of the HMS quadrupoles at the low momentum. After the new HMS power supplies were installed in the summer of 2021, all the HMS magnets and their power supplies were studied at momentum of 125, 250, 500, 1000, 2500, 4000 and 5500 MeV/c. For the lowest momentum setting of the experiment (388 MeV/c), the HMS Q3 is at the lowest current of 19A with Q1 and Q2 at 40A and 50A. Down to 250 MeV/c , the Q3 readback current was consistent with the set current at 0.01% level.

Furthermore, the HMS was operated to momentum of 440 MeV/c during an experiment that acquired data in the summer 2019 running period. The sieve slit data showed the expected resolution effects from multiple scattering, and the focal plane distribution did not show a change when the momentum changed from 1 GeV/c to 0.44 GeV/c. This indicates that the optics of the HMS scale properly and reliably at the $\sim$ 400 MeV/c range. If need be, we can adjust the lowest momentum setting from 388 MeV/c to a similar momentum range above 400 MeV/c. Here, we note that the lowest momentum of the 388 (MeV/c) involves only one of the 28 kinematical settings of the proposal. The other 27 settings are above 400 (MeV/c) and involve gradually increasing momenta. If the lowest momentum setting (388 MeV/c) was to be adjusted to a higher momentum, the impact to the projected results of the experiment would be inconsiquential.

We have performed studies to identify the effect of the systematic uncertainties on the results, including resolution effects due to the low momentum settings. We have determined that the systematic uncertainty in the cross section measurements will be ranging at the $\sim 3\% - 4\%$ range, depending on the kinematics.

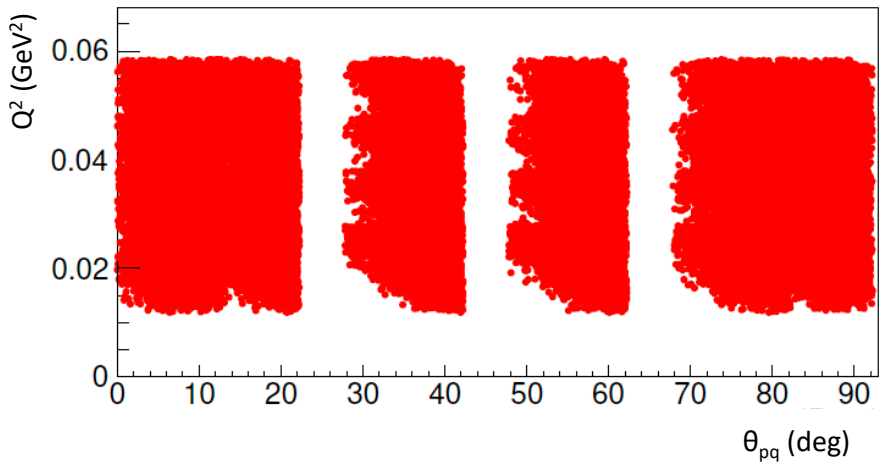

Figure 10. The phase space that will be accessed by the proposed measurements, after a first layer of acceptance cuts and phase space masking has been applied.

These uncertainties have been taken under consideration in the extraction of the $N \rightarrow \Delta$ TFFs. Furthermore, the experiment plans to take sieve data with singles electrons at 575, 480 and 388 MeV/c as a check on the optics. In addition, elastic ep coincidence data will be taken at the same momentum settings as a check on the delta optics. This can also be studied with the π^0 production data.

Lastly, in regards to the 1.3 GeV/c beam energy, Jay Benesch and Yves Roblin estimate that the accelerator would need one or two days for a dedicated one hall setup for this energy, if a dedicated one hall running is required. In such a case, the accelerator/hall uptime efficiency can be estimated at 67% rather than the usual 50%, thus expediting notably the experiment running period.

3.2 Kinematical Settings

The kinematical settings are summarized in Table 1. The SHMS spectrometer will be set to access a range of Q^2 settings sequentially. For each one of these settings, the HMS spectrometer will in-turn measure an extended phase space through a series of sub-set measurements. The kinematical phase space that will be accessed by the proposed measurements is shown in Fig. 10, after a first layer of acceptance cuts and phase space masking has been applied. A second layer of cuts will further bin the phase space in Q^2 and in θ^*_{pq}, as shown in Fig. 12. The beam current for the settings in groups *b, c,* and *d* will be 15 μA. For the settings in group-*a* the beam current will be set to 6 μA so that the SHMS rate can stay below the 1 MHz level (note: during the summer 2019 running period, we were able to operate the SHMS spectrometer at the 1.3 MHz rate without any concern; these measurements employed a similar configuration (E12-15-001 experiment) to the configuration of the current proposal). For the lowest Q^2 setting, the uncertainty of the beam charge determination will increase from 1% to 2%. The HMS singles rate is at a comfortable level of a few tens of KHz for all the settings, as shown in Table 2. These rates have been calculated using the well established Wiser calculations for pions and protons, and the Bosted inelastic calculation folded with the SHMS acceptance for electron-singles. The signal-to-noise ratio (S/N), within a coincidence timing window of 1.5 ns, ranges between 1.2 and 7, as given in Table 1. Further suppression of accidentals can be achieved by applying a missing mass cut in the data analysis.

Setting	SHMS θ (deg)	SHMS P (MeV/c)	HMS θ (deg)	HMS P (MeV/c)	S/N	Time (hrs)
1a			18.77	532.53	2	7
2a			25.17	527.72	2	7
3a			33.7	506.61	3.2	6
4a	7.29	952.26	42.15	469.66	4.3	5
5a			50.44	418.56	4.9	5
6a			54.47	388.38	4.9	5
7a			12.37	527.72	2.7	6
1b			22.01	547.54	1.2	6
2b			28.24	542.61	1.4	6
3b			36.52	520.95	2.5	5
4b	8.95	946.93	44.64	483.08	3.4	4
5b			52.68	430.78	3.7	4
6b			56.53	399.92	3.5	4
7b			12.46	535.98	1.6	5
1c			24.40	562.00	1.5	9
2c			30.47	556.95	1.9	9
3c			38.52	534.79	3.5	6
4c	10.37	941.61	46.47	496.06	4.4	6
5c			54.17	442.64	4.8	6
6c			57.85	411.16	4.8	6
7c			12.69	543.24	2	6
1d			26.24	575.96	1.8	12
2d			32.16	570.80	2.5	11
3d			40.01	548.17	4.5	8
4d	11.63	936.28	47.73	508.64	5.5	8
5d			55.18	454.17	6.9	7
6d			58.71	422.13	6	8
7d			12.47	548.17	2.1	10

Table 1. The kinematical settings of the proposed measurements, utilizing an 1.3 GeV beam. The signal-to-noise ratio and the required beam time are given for each setting.

Setting	SHMS e^- (KHz)	SHMS π^-(KHz)	HMS p (KHz)	HMS π^+ (KHz)
1a	970.2	5.04	5.1	25.6
2a			5.6	23.5
3a			5.3	19.1
4a			4.3	15.9
5a			3.2	14.8
6a			2.6	15.1
7a			4.0	23.8
1b	885.1	11.5	11.6	49.7
2b			11.8	42.7
3b			10.4	33.3
4b			8.2	27.7
5b			5.8	26.2
6b			4.7	27.3
7b			8.4	49.3
1c	510.0	12.0	11.9	45.3
2c			11.6	37.3
3c			9.8	28.4
4c			7.5	23.5
5c			5.2	22.9
6c			4.1	24.2
7c			8.6	49.1
1d	331.1	12.3	11.9	40.9
2d			11.2	32.8
3d			9.2	24.6
4d			6.9	20.5
5d			4.7	20.3
6d			3.6	21.7
7d			8.6	48.7

Table 2. Singles rates for the SHMS and the HMS spectrometers.

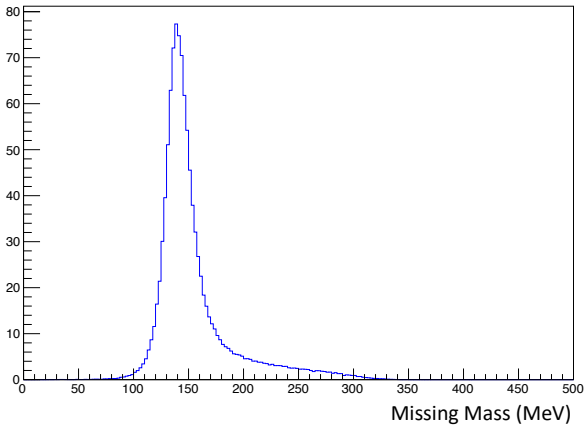

Figure 11. The missing mass spectrum, corresponding to the undetected pion.

3.3 Data analysis and projected results

The cross section of the $p(e,e'p)\pi^\circ$ reaction is sensitive to a set of independent partial responses $(\sigma_T, \sigma_L, \sigma_{LT}, \sigma_{TT})$:

$$\frac{d^5\sigma}{d\omega d\Omega_e d\Omega^{cm}_{pq}} = \Gamma(\sigma_T + \varepsilon\cdot\sigma_L - v_{LT}\cdot\sigma_{LT}\cdot\cos\phi^*_{pq} + \varepsilon\cdot\sigma_{TT}\cdot\cos 2\phi^*_{pq})$$

where $v_{LT} = \sqrt{2\varepsilon(1+\varepsilon)}$ is a kinematic factor, ε is the transverse polarization of the virtual photon, Γ is the virtual photon flux, and ϕ^*_{pq} is the proton azimuthal angle with respect to the electron scattering plane. The differential cross sections $(\sigma_T, \sigma_L, \sigma_{LT}, \sigma_{TT})$ are all functions of the center-of-mass energy W, the Q^2, and the proton center of mass polar angle θ^*_{pq} that is measured from the momentum transfer direction. The $\sigma_0 = \sigma_T + \varepsilon\cdot\sigma_L$ response is dominated by the $M1$ resonant multipole while the interference of the $C2$ and $E2$ amplitudes with the $M1$ dominates the Longitudinal - Transverse and Transverse - Transverse responses, respectively. Cross section measurements will be performed at the nucleon resonance region, extending from $Q^2 = 0.015\ (GeV/c)^2$ to $Q^2 = 0.055\ (GeV/c)^2$. The measurements will cover a θ^*_{pq} range from 0° to 90°. They will be conducted at in-plane kinematics, with the spectrometer acceptance offering an out-of plane ϕ^*_{pq} access up to 30°. For part of the θ^*_{pq} kinematical coverage (due to space limitations of the experimental setup) it will become possible to position the proton spectrometer symmetrically at $\phi^*_{pq} = 0^\circ$ and at 180°. Thus it will become possible to measure the in-plane azimuthal asymmetry of the cross section, with respect to the momentum transfer direction, $A_{(\phi_{pq}=0,\pi)} = [\sigma_{\phi_{pq}=0} - \sigma_{\phi_{pq}=180}]/[\sigma_{\phi_{pq}=0} + \sigma_{\phi_{pq}=180}]$. This will in-turn enhance the sensitivity to the measurement of the Coulomb quadrupole amplitude. In this case, for the pair of $\phi^*_{pq} = 0^\circ$ and 180° measurements, the cross sections and asymmetries will be obtained with the phase space matched in (W,Q^2,θ^*_{pq}). A first level of acceptance cuts will be applied in the data analysis aiming to limit the phase space to the central region of the spectrometers and to ensure that potential edge effects will be avoided. It will be followed by a second layer of analysis cuts where the phase space will be further binned. Point cross sections will be extracted from the finite acceptances by utilizing the cross section calculations from the state of the art theoretical models[26–28,44,45] in the Monte Carlo simulation. Radiative corrections, energy losses and resolution effects will be integrated in the data analysis using the Monte Carlo simulation. The reconstructed missing mass spectrum is shown in Fig. 11. Our studies on the effect of the systematic uncertainties have been based on Monte Carlo simulation studies and on the standard performance of the experimental setup. For the measured cross section, the overall systematic uncertainties will range from 2.8% to 4%, depending on the kinematics. They will

Resolution	2% - 3%
Acceptance	1%
Scattering angle	0.4% - 0.6%
Beam energy	0.7% - 1.2%
Beam charge	1% - 2%
Target density	0.5%
Detector efficiencies	0.5%
Target cell background	0.5%
Target length	0.5%
Dead-time corrections	0.5%
Total	2.8% - 4.0%

Table 3. Summary table of the cross section systematic uncertainties.

be dominating over the $\sim 1\%$ statistical uncertainty of the cross section measurements. The systematic uncertainties are driven by the level of understanding of the acceptance, the resolution of the experimental setup, the uncertainty of the beam energy and of the scattering angle, the beam charge determination, and to a smaller extent by the target density, detector efficiencies, target cell background, target length and dead time corrections. A break-down of the systematic uncertainties is given in Table 3. For the asymmetry measurements, the systematic uncertainties will be further suppressed through the cross section ratio. A second advantage emerges here, since the electron spectrometer position and momentum settings do not change during the asymmetry measurements. The projected level of systematic uncertainties is equivalent to the one demonstrated in measurements that were performed in the past, with similar experimental setups at JLab and at MAMI [21,23,31,36].

For the extraction of the resonant amplitudes from the measured cross sections, consideration has to be given in the treatment of the non-resonant pion electro-production amplitudes that interfere with the resonant amplitudes in the $N \rightarrow \Delta$ transition. These interfering contributions, small in magnitude but large in number, can not be sufficiently constrained by the experimental measurements, and they thus result into a model uncertainty for the quadrupole transition form factors. In the past these contributions have been occasionally poorly studied or quoted as an uncertainty. Here, the effect of these amplitudes is studied by employing in the data analysis state of the art theoretical pion electroproduction models[26–28,44,45]. Fits of the resonant amplitudes will be performed while taking into account the contributions of background amplitudes from the different models. The models offer different descriptions for the background amplitudes, leading to deviations in the extracted values of the transition form factors that are quantified as a model uncertainty. This procedure has been followed in the past in various experiments e.g.[21,23,31,36]. The good level of control over the model uncertainties has been further validated experimentally, with measurements of the weak $p(e,e'p)\gamma$ excitation channel. In this case, one extracts the same physics signal within a different theoretical framework. This offers an ideal cross-check to the model uncertainties associated with the pion electroproduction channel. The branching ratio of the photon channel is very small (0.6%), two orders of magnitude smaller compared to the pion-electroproduction, and as such it was not studied until recently. To that end, the first such measurement was conducted at MAMI[24]. Measurements for both channels were performed at the same Q^2 and used the same experimental setup. The results were found in very good agreement between the two channels[24,31], thus giving credence to the quantification of the model uncertainties that are derived following the procedure that is described above.

With data that were acquired recently in Hall C, we were able to demonstrate the readiness of the experimental and theoretical tools that will be used in the proposed measurements. More specifically,

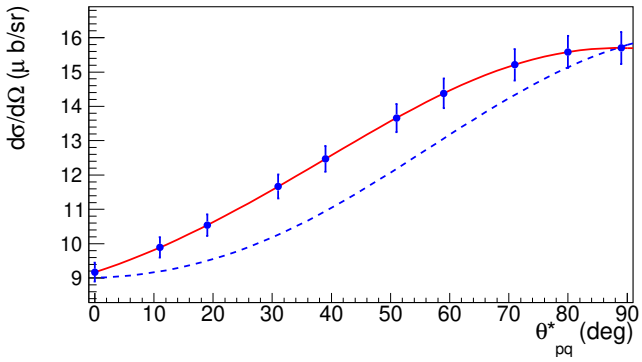

Figure 12. Projected cross section measurements at $Q^2 = 0.02\ (GeV/c)^2$ and $\phi^*_{pq} = 180°$. The solid line shows the MAID cross section (C2/M1=-4.5%). The dashed line shows the cross section prediction for C2=0.

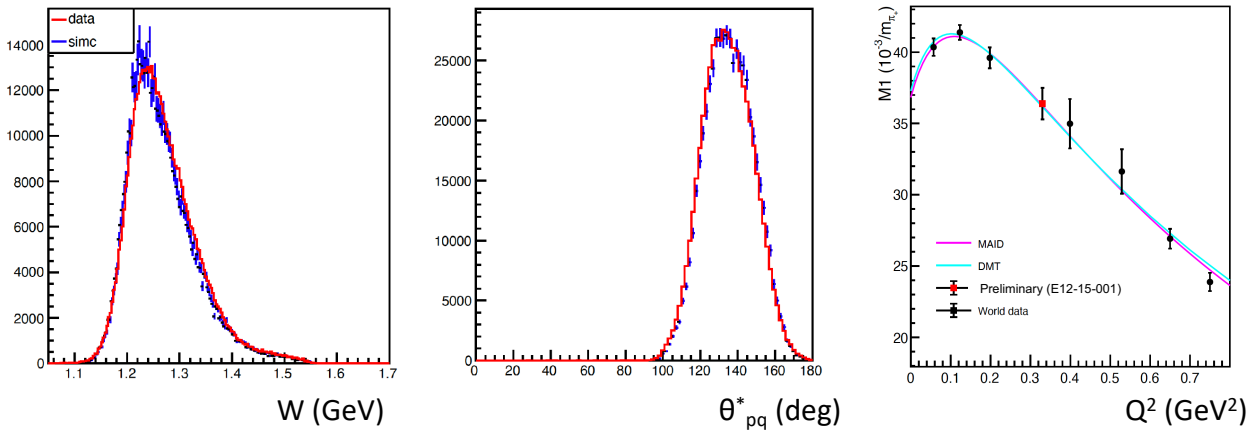

Figure 13. The measurement of the $p(e,e'p)\pi^\circ$ reaction at $Q^2 = 0.33\ (GeV/c)^2$ during the E12-15-001 (VCS) experiment, using the same experimental arrangement (SHMS and HMS) that will be used in this proposal. Left and center: The data are compared to the experiment simulation (weighted with the MAID cross section). Right: The preliminary extraction of the M1 transition form factor at $Q^2 = 0.33\ GeV^2$.

we had the opportunity to measure the $p(e,e'p)\pi^\circ$ reaction channel, parasitically during the running of the E12-15-001 (VCS) experiment. The measurements utilized the same experimental setup that is proposed here (i.e. SHMS and HMS measured electrons and protons in coincidence, respectively). The measurements were conducted at a slightly higher momentum transfer of $Q^2 = 0.3\ (GeV/c)^2$ where the cross section of the reaction is well known. The cross section results demonstrate that we have an excellent understanding of the coincidence acceptance in the simulation of the experiment, a good handle of the systematic uncertainties, and validate the readiness of all the experimental and theoretical tools involved in the analysis of the proposed measurements. In Fig. 13, the data are compared to the simulation. The data have been corrected for all known efficiencies, and no arbitrary normalization factor has been applied in the analysis. The simulation has been weighted with the MAID cross section, which is known to describe the data very well in this kinematical region. The extraction of the dominant magnetic dipole (M1) transition form factor is also shown in Fig. 13 and it is compared to the world data.

The projected measurements for the two quadrupole amplitudes are shown in Fig. 14. In Fig. 15 the

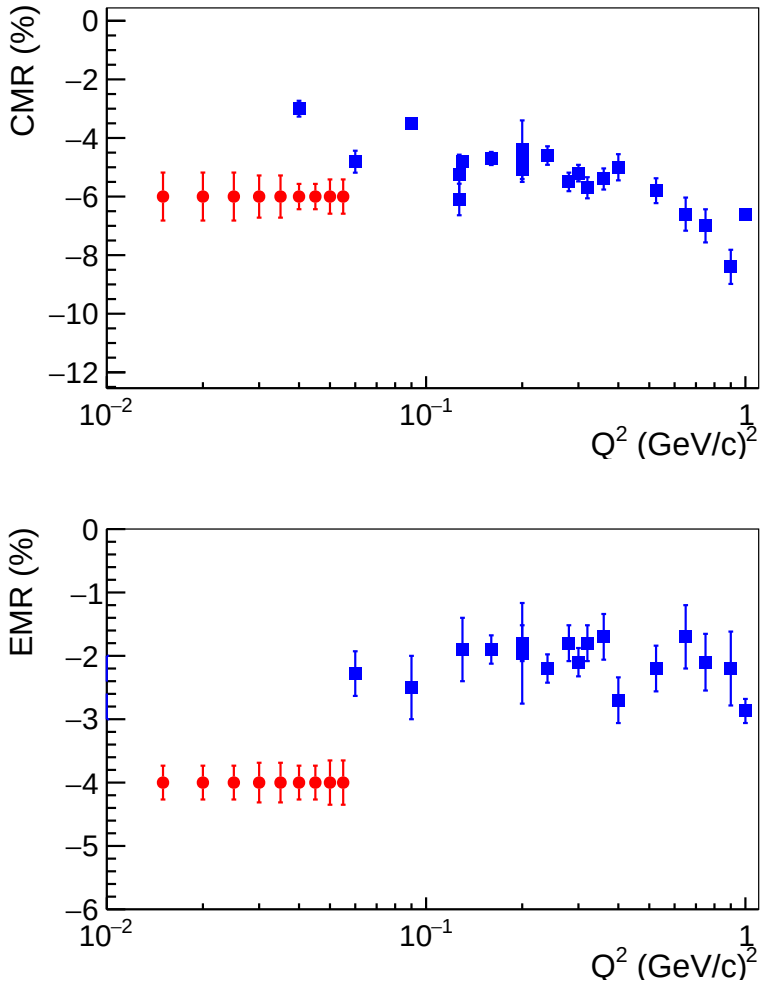

Figure 14. The projected CMR and EMR measurements (red) and the world data (blue).

projected data are compared to a wide spectrum of theoretical calculations, namely that of MAID[28,44], DMT[27], SAID[45], the ChEFT of PV[40], the Sato-Lee[26], GH[41], Large-Nc[46], DSEM[47] and the constituent quark models of Capstick[7] and HQM[42]. The comparison emphasizes the strong constraints and new input that the new measurements will provide to the theory.

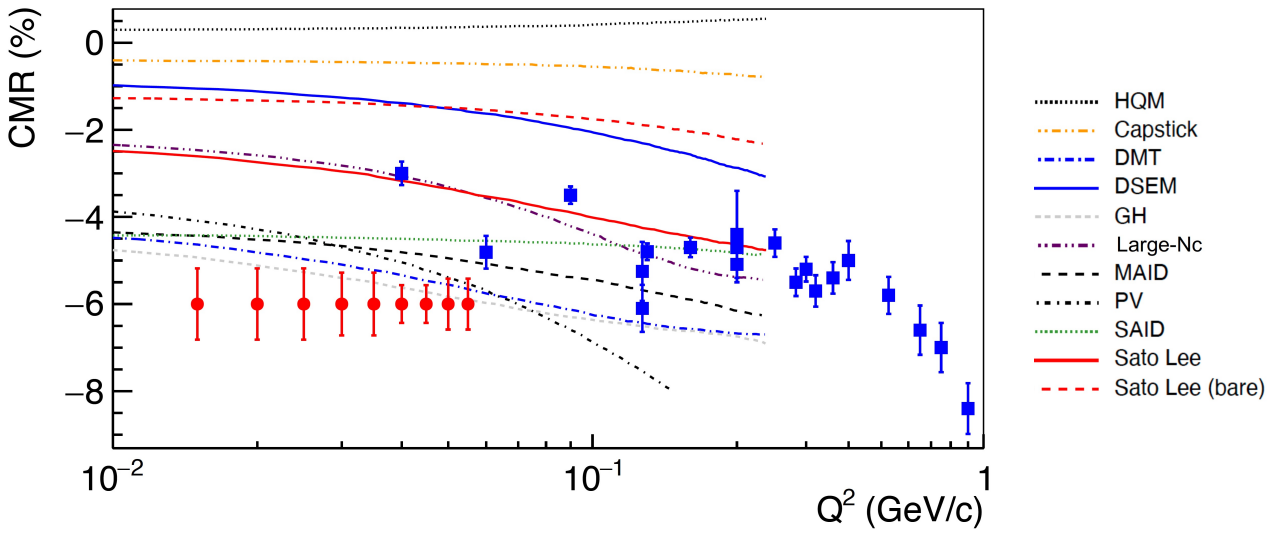

Figure 15. The theoretical predictions of MAID[28,44], DMT[27], SAID[45], PV[40], Sato-Lee[26], GH[41], Large-Nc[46], DSEM[47], Capstick[7] and HQM[42] are compared to the projected measurements (red points) and to the world data.

4 Summary

The first excited state of the nucleon holds a prominent role in the physics of the strong interaction and as such it has been a central part of Jefferson Lab's experimental program. In this work we will extend this physics program and we will explore key aspects of the nucleonic structure that are essential in order to decode the dynamics of the system. We will conduct a precise study of the mesonic cloud dynamics in a region where they are dominant and rapidly changing. We will perform measurements of the quadrupole TFFs that have emerged as the experimental signature for the presence of non-spherical components in the nucleon wavefunction, aiming to decode the underlying system dynamics, and will provide benchmark data that will offer a test bed for chiral effective field theory calculations and lattice QCD calculations. The proposed measurements will make possible a test to the theoretical prediction that the Electric and the Coulomb quadrupole amplitudes converge as $Q^2 \to 0$. Beyond the direct benefit in our understanding of the baryon structure, the new data for the TFFs will serve as an input in a number of scientific topics ranging from the hadronic to neutrino physics, thus extending the impact and the scientific merit of the proposed measurements across different domains of nuclear and particle physics.

The experiment will require standard Hall C equipment, namely a 4 cm liquid hydrogen target, an 1.3 GeV beam with $I = 15\ \mu A$, and the SHMS and the HMS spectrometers with their standard detector packages, for the measurement of electrons and protons, respectively. The experiment will need to acquire data for 11 days at full efficiency (corresponding to 8 days for production and 3 days for optics, normalization and dummy measurements) so that it can provide the most precise measurement of the $N \to \Delta$ TFFs in the low-Q^2 region, down to 0.01 GeV^2.

References

1. A. de Rujula, H. G. & Glashow, S. *Phys. Rev. D* **12**, 147 (1975).
2. Glashow, S. *Physica* **96A**, 27 (1979).
3. Bernstein, A. & Papanicolas, C. Shapes of hadrons. *AIP. Conf. Proc.* **904**, 1 (2007).
4. Alexandrou, C., Papanicolas, C. & Vanderhaeghen, M. *Rev. Mod. Phys.* **84**, 1231 (2012).
5. Bernstein, A. *Eur. Phys. J. A* **17**, 349 (2003).
6. N. Isgur, G. K. & Koniuk, R. *Phys. Rev.* **D25**, 2394 (1982).
7. Capstick, S. & Karl, G. *Phys. Rev.* **D41**, 2767 (1990).
8. Blanpied, G. *Phys. Rev. Lett.* **79**, 4337 (1997).
9. Beck, R. *et al. Phys. Rev. Lett.* **78**, 606 (1997).
10. Beck, R. *et al. Phys. Rev.* **C61**, 035204 (2000).
11. Frolov, V. *et al. Phys. Rev. Lett.* **82**, 45 (1999).
12. Pospischil, T. *et al. Phys. Rev. Lett.* **86**, 2959 (2001).
13. Mertz, C. *et al. Phys. Rev. Lett.* **86**, 2963 (2001).
14. Bartsch, P. *et al. Phys. Rev. Lett.* **88**, 142001 (2002).
15. van Buuren, L. *et al. Phys. Rev. Lett.* **89**, 012001 (2002).
16. van Buuren, L. *et al. Phys. Rev. C* **70**, 042201 (2004).
17. Kunz, C. *et al. Phys. Lett. B.* **564**, 21 (2003).
18. Sparveris, N. F. *et al.* Investigation of the conjectured nucleon deformation at low momentum transfer. *Phys. Rev. Lett.* **94**, 022003 (2005).
19. Kelly, J. *Phys. Rev. Lett.* **95**, 102001 (2005).
20. Kelly, J. J. *et al.* Recoil polarization measurements for neutral pion electroproduction at $Q^2 = 1$ $(GeV/c)^2$ near the Delta resonance. *Phys. Rev.* **C75**, 025201 (2007).
21. Stave, S. *et al.* Lowest Q^2 Measurement of the $\gamma*$ p —> Δ Reaction: Probing the Pionic Contribution. *Eur. Phys. J.* **A30**, 471–476 (2006).
22. Ungaro, M. *et al. Phys. Rev. Lett.* **97**, 112003 (2006).
23. Blomberg, A. *et al.* Electroexcitation of the $\Delta^+(1232)$ at low momentum transfer. *Phys. Lett.* **B760**, 267–272 (2016).
24. Blomberg, A. *et al.* Virtual Compton Scattering measurements in the nucleon resonance region. *Eur. Phys. J. A* **55**, 182 (2019). 1901.08951.
25. Alexandrou, C. *et al. Phys. Rev. Lett.* **94**, 021601 (2005).
26. Sato, T. & Lee, T. Dynamical study of the Delta excitation in N (e, e-prime pi) reactions. *Phys. Rev. C* **63**, 055201 (2001).
27. Kamalov, S. & Yang, S. N. Pion cloud and the Q^2 dependence of $\gamma*$ N <—> Δ transition form-factors. *Phys. Rev. Lett.* **83**, 4494–4497 (1999).
28. Kamalov, S., Chen, G.-Y., Yang, S.-N., Drechsel, D. & Tiator, L. Pi0 photoproduction and electroproduction at threshold within a dynamical model. *Phys. Lett. B* **522**, 27–36 (2001).

29. SAID. http://gwdac.phys.gwu.edu.

30. Elsner, D. *et al.* Measurement of the LT-asymmetry in π^0 electroproduction at the energy of the $\Delta(1232)$ resonance. *Eur. Phys. J.* **A27**, 91–97 (2006).

31. Sparveris, N. F. *et al.* Determination of quadrupole strengths in the $\gamma * p \to \Delta(1232)$ transition at $Q^2 = 0.20\ (GeV/c)^2$. *Phys. Lett.* **B651**, 102–107 (2007).

32. Stave, S. *et al. Phys. Rev. C* **78**, 024209 (2008).

33. Aznauryan, I. G. *et al.* Electroexcitation of nucleon resonances from CLAS data on single pion electroproduction. *Phys. Rev.* **C80**, 055203 (2009).

34. Villano, A. N. *et al. Phys. Rev. C* **80**, 035203 (2009).

35. van Buuren, L. *et al. Phys. Rev. C* **84**, 028201 (2011).

36. Sparveris, N. *et al.* Measurements of the γ*p $\to \Delta$ reaction at low Q^2. *Eur. Phys. J.* **A49**, 136 (2013).

37. D.-H. Lu, A. W. T. & Williams, A. G. *Phys. Rev. C* **55**, 3108 (1997).

38. U. Meyer, E. H. & Buchmann, A. J. *Phys. Rev. C* **64**, 035203 (2001).

39. M. Fiolhais, B. G. & Sirca, S. *Phys. Lett. B* **373**, 229 (1996).

40. Pascalutsa, V. & Vanderhaeghen, M. *Phys. Rev. D* **73**, 034003 (2006).

41. Gail, T. A. & Hemmert, T. R. *Eur. Phys. J A* **28**, 91 (2006).

42. Sanctis, M. D. *et al. Nucl. Phys. A* **755**, 294 (2005).

43. Mandeville, J. *et al. Phys. Rev. Lett.* **72**, 3325 (1994).

44. Drechsel, D., Hanstein, O., Kamalov, S. S. & Tiator, L. A Unitary isobar model for pion photoproduction and electroproduction on the proton up to 1-GeV. *Nucl. Phys.* **A645**, 145–174 (1999).

45. Arndt, R. A., Briscoe, W. J., Strakovsky, I. I. & Workman, R. L. Analysis of pion photoproduction data. *Phys. Rev.* **C66**, 055213 (2002).

46. Pascalutsa, V. & Vanderhaeghen, M. *Phys. Rev. D* **76**, 111501 (2007).

47. Segovia, J. *et al. Few-Body Syst.* **55**, 1185–1222 (2014).

48. Tiator, L. *et al. Eur. Phys. J. A* **17**, 357 (2003).

49. Isgur, N. & Karl, G. *Phys. Rev. D* **18**, 4187 (1978).

50. Rujula, A. D., Georgi, H. & Glashow, S. L. *Phys. Rev. D* **12**, 147 (1975).

51. Rujula, A. D., Georgi, H. & Glashow, S. L. *Phys. Rev. D* **21**, 1868 (1980).

52. Isgur, N., Karl, G. & Koniuk, R. *Phys. Rev. D* **25**, 2394 (1982).

53. Kaelbermann, G. & Eisenberg, J. M. *Phys. Rev. D* **28**, 71 (1983).

54. K. Bermuth, L. T., D. Drechsel & Seaborn, J. B. *Phys. Rev. D* **37**, 89 (1988).

55. Wirzba, A. & Weise, W. *Phys. Lett. B* **188**, 6 (1987).

56. Walliser, H. & Holzwarth, G. *Z. Phys. A* **357**, 317 (1997).

57. Watabe, T., Christov, C. V. & Goeke, K. *Phys. Lett. B* **349**, 197 (1995).

58. Buchmann, A. J., Hernandez, E. & Faessler, A. *Phys. Rev. C* **55**, 448 (1997).

59. 't Hooft, G. *Nucl. Phys. B* **72**, 461 (1974).

60. Witten, E. *Nucl. Phys. B* **160**, 57 (1979).

61. Jenkins, E. *Ann. Rev. Nucl. Part. Sci.* **48**, 81 (1998).

62. Jenkins, E. *Czech. J. Phys.*. **49**, 1273 (1999).

63. Jenkins, E. & Manohar, A. V. *Phys. Lett. B* **335**, 452 (1994).

64. E. Jenkins, X. d. J. & Manohar, A. V. *Phys. Rev. Lett.* **89**, 242001 (2002).

65. A. J. Buchmann, J. A. H. & Lebed, R. F. *Phys. Rev. D* **66**, 056002 (2002).

66. Pascalutsa, V. & Vanderhaeghen, M. *Phys. Rev. D* **76**, 111501 (2007).

67. Grabmayr, P. & Buchmann, A. J. Moments of the neutron charge form-factor and the N —> Δ quadrupole transition. *Phys. Rev. Lett.* **86**, 2237–2240 (2001).

68. Alexandrou, C. *et al. Phys. Rev. D* **83**, 014501 (2011).

69. Alexandrou, C. University of Cyprus, Extended Twisted Mass Collaboration, private communication (2022).

70. Alexandrou, C. *et al. arXiv:2112.04146* (2011).

71. Alexandrou, C. *et al. Phys. Rev. D* **98**, 074502 (2018).

72. Alexandrou, C. *et al. Phys. Rev. D* **66**, 094503 (2002).

73. Alexandrou, C. *et al. Phys. Rev. D* **79**, 014507 (2009).

74. M. N. Butler, M. J. S. & Springer, R. P. *Phys. Lett. B* **304**, 353 (1993).

75. G. C. Gellas, C. N. K., T. R. Hemmert & Poulis, G. I. *Phys. Rev. D* **60**, 054022 (1999).

76. Gail, T. A. & Hemmert, T. R. *Eur. Phys. J. A* **28**, 91 (2006).

77. Pascalutsa, V. & Phillips, D. R. *Phys. Rev. C* **67**, 055202 (2003).

78. Pascalutsa, V. & Vanderhaeghen, M. *Phys. Rev. Lett.* **95**, 232001 (2005).

79. Carlson, C. & Vanderhaeghen, M. *Phys. Rev. Lett.* **100**, 032004 (2008).

80. Atac, H. *et al.* Measurement of the neutron charge radius and the role of its constituents. *Nature Communications* **12**, 1759 (2021).

81. Fernando, I. & Goity, J. *Phys. Rev. D* **101**, 054026 (2020).

82. Fonvieille, H., Pasquini, B. & Sparveris, N. *Prog. Part. Nucl. Phys.* **113**, 103754 (2020).

83. Laveissiere, G. *et al. Phys. Rev. Lett.* **93**, 122001 (2004).

84. Fonvieille, H. *et al. Phys. Rev. C.* **86**, 015210 (2012).

85. Pasquini, B. *et al. Phys. Rev. C.* **62**, 052201(R) (2000).

86. Pasquini, B., Gorchtein, Drechsel, D., Metz, A. & Vanderhaeghen, M. *Eur. Phys. J. A* **11**, 185 (2001).

87. Drechsel, D., Pasquini, B. & Vanderhaeghen, M. *Phys. Rep.* **378**, 99 (2003).

88. Nakamura, S. *et al. Rep. Prog. Phys.* **80**, 056301 (2017).

89. Nakamura, S., Kamano, H. & Sato, T. *Phys. Rev. D* **92**, 074024 (2015).